Review, Role of $L1_2$ Modified $(Al_{1-x}Me_x)_3Ti$ Intermetallic Compounds on Heterogeneous Nucleation of Alpha Aluminum Grains

Yoshimi Watanabe*

Department of Physical Science and Engineering, Nagoya Institute of Technology, Gokiso-cho, Showa-ku, Nagoya, Japan

Abstract. Al_3Ti intermetallic compound with the tetragonal $D0_{22}$ structure undergoes a phase transformation to the high-symmetry $L1_2$ cubic structure by addition of third elements, *Me*. The lattice constants of some $L1_2$ modified $(Al_{1-x}Me_x)_3Ti$ intermetallic compounds are closed to that of alpha aluminum. Therefore, it is expected that the addition of $L1_2$ modified $(Al_{1-x}Me_x)_3Ti$ intermetallic compound particles show good grain refining performance of cast aluminum. In this paper, our recent results on novel refines containing heterogeneous nucleation site particles of $L1_2$ modified $(Al_{1-x}Me_x)_3Ti$ intermetallic compounds have been reviewed.

1 INTRODUCTION

Equiaxed grain structure ensures uniform mechanical properties, reduced ingot cracking, improved feeding to eliminate shrinkage porosity, distribution of secondary phases and microporosity on a fine scale, improved machinability and cosmetic features. The grain refining innoculants commonly used in the aluminium industry are usually master alloys of A1-Ti or A1-Ti-B [1]. Grain refinement of aluminum and its alloys by the addition of Al-Ti-B refiners to liquid melt prior to casting is a common practice in order to achieve a fine equiaxed grained microstructure in a casting which otherwise solidifies usually with coarse columnar grain structure [2]. Figure 1 shows microstructural feature of Al-Ti-B refiner. As can be seen, the Al-Ti-B refiner contains TiB_2 heterogeneous nucleation site particles and platelet-shaped Al_3Ti heterogeneous nucleation site particles [3-8] with $D0_{22}$ structure (a = 0.3851 nm, c = 0.8608 nm). It is well accepted that the effective heterogeneous nucleation site particles have better lattice matching with the solidified alpha aluminium (a = 0.4049 nm).

It is also known that the Al_3Ti intermetallic compound with the tetragonal $D0_{22}$ structure can undergo a phase transformation into $(Al_{1-x}Me_x)_3Ti$ intermetallic compounds with $L1_2$ cubic structure by addition of third elements of *Me* [9-11]. Moreover, the lattice constant of some $L1_2$ modified $(Al_{1-x}Me_x)_3Ti$ intermetallic compounds is closed to that of alpha aluminum, *e.x.*, the lattice constants of $L1_2$ modified $Al_{2.7}Fe_{0.3}Ti$, $Al_{2.75}Ni_{0.25}Ti$ and $Al_{2.5}Cu_{0.5}Ti$ intermetallic compounds are a = 0.393 nm, a =0.394 nm and a = 0.3927 nm, respectively. An $L1_2$ modified $Al_{2.5}Cu_{0.5}Ti$ intermetallic compound can be formed at the Cu/Al_3Ti interface in the Cu/Al_3Ti diffusion couple specimen heated at elevated temperature as shown in Fig. 2 [12].

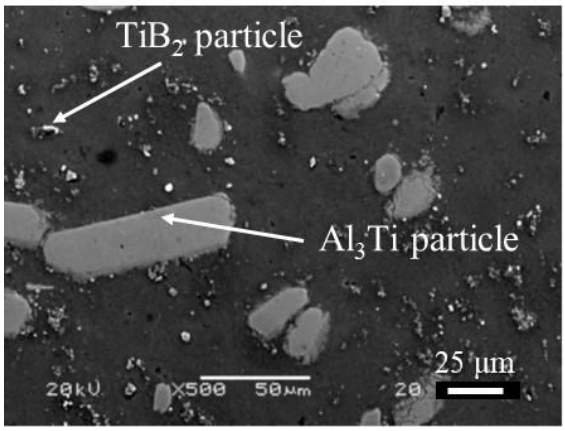

Fig. 1. SEM micrograph of Al-Ti-B refiner.

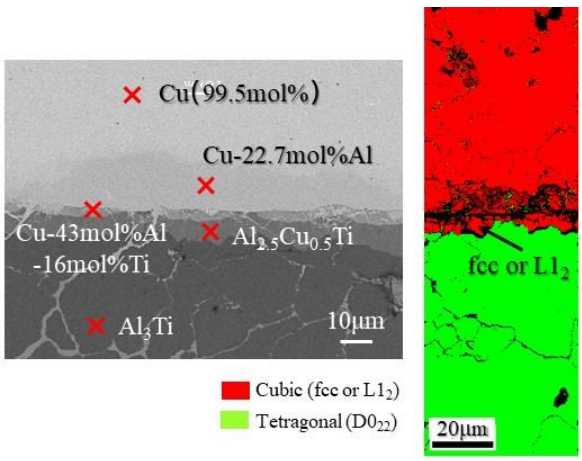

Fig. 2. Micrographs showing the interface in the Cu/Al_3Ti diffusion couple specimen heated at 600 °C for 4 h [12].

* Corresponding author: yoshimi@nitech.ac.jp

Therefore, it is expected that these intermetallic compounds show good grain refining performance. In our studies [13-17], refining performance of novel refines with $L1_2$ modified $Al_{2.5}Cu_{0.5}Ti$, $Al_{2.7}Fe_{0.3}Ti$ and $Al_{2.7}Ni_{0.3}Ti$ particles are studied. In this paper, our recent results on novel refines containing heterogeneous nucleation site particles of $L1_2$ modified $(Al_{1-x}Me_x)_3Ti$ intermetallic compounds have been reviewed.

2 LATTICE MATCHING

It is important to describe the lattice matching between heterogeneous nucleation site particles and alpha aluminum, because an effective refiner contains heterogeneous nucleation site particles with a better lattice matching with the solidified phase. One of the most famous equations is eq. (1) proposed by Turnbull and Vonnegut [18].

$$\delta = (|a_S - a_C| / a_C) \times 100(\%) \qquad (1)$$

where δ is called as disregistry between the heterogeneous nucleation site and the solidified phase, a_S and a_C are the lattice parameters of the heterogeneous nucleation site particles and solidified phase without deformation, respectively. However, Al_3Ti has the low-symmetry tetragonal $D0_{22}$ structure. Therefore, eq. (1) must be modified for application to two-dimensional lattices. The plane disregistry was proposed by Bramfitt [19], and calculated by

$$\delta_{(hkl)_n}^{(hkl)_s} = \frac{1}{3}\sum_{i=1}^{3}\left\{\left|d[uvw]_s^i \cos\theta - d[uvw]_n^i\right| \Big/ d[uvw]_n^i\right\} \times 100\% \qquad (2)$$

where $(hk\lambda)_s$ and $(hk\lambda)_n$ are the low-index planes of the heterogeneous nucleation site and solidified phase, and $[uvw]_s$ and $[uvw]_n$ are the low-index orientations on $(hk\lambda)_s$ and $(hk\lambda)_n$, respectively. Moreover, $d[uvw]_s$ and $d[uvw]_n$ are the interatomic spacing distances along $[uvw]$, and θ is the angle between $[uvw]_s$ and $[uvw]_n$.

However, it is unclear why three in-plane directions are considered when evaluating the plane disregistry. Moreover, there are some possibilities to select the third axis [15]. Kato *et al.* have proposed parameter *M* [20], which is approximately proportional to the specific misfit strain energy. In this study, parameter *M* defined by eq. (3) will be adopted to discuss the effective heterogeneous nucleation site [21,22].

$$M = \varepsilon_1^2 + \varepsilon_2^2 + (2/3)\varepsilon_1\varepsilon_2, \qquad (3)$$

In eq. (3), ε_1 and ε_2 are the principal misfit strains calculated from the principal distortions. The parameter *M* values of some crystallographic orientation relationships between Al_3Ti and aluminum are listed in Table 1. As can be seen, different planes of Al_3Ti show different parameter *M* values. In case of $L1_2$ modified $(Al_{1-x}Me_x)_3Ti$ intermetallic compounds, better lattice matching between the heterogeneous nucleation sites and the solidified phase can be achieved, as shown in Table 1.

Table 1. Parameter *M* values between heterogeneous nucleation site particles and aluminum.

Orientation Relationship	*M* value
$(100)_{Al_3Ti}$ // $(100)_{Al}$	4.31 x 10^{-3}
$(001)_{Al_3Ti}$ // $(100)_{Al}$	6.38 x 10^{-3}
$(110)_{Al_3Ti}$ // $(110)_{Al}$	4.31 x 10^{-3}
$(112)_{Al_3Ti}$ // $(111)_{Al}$	2.24 x 10^{-3}
$(0001)_{TiB_2}$ // $(111)_{Al}$	9.95x 10^{-3}
$(hk\lambda)_{Al_{2.5}Cu_{0.5}Ti}$ // $(hk\lambda)_{Al}$	2.57 x 10^{-3}
$(hk\lambda)_{Al_{2.7}Fe_{0.3}Ti}$ // $(hk\lambda)_{Al}$	2.50 x 10^{-3}
$(hk\lambda)_{Al_{2.7}Ni_{0.3}Ti}$ // $(hk\lambda)_{Al}$	1.93 x 10^{-3}

3 EXPERIMENTAL METHODS

3.1 Fabrication of Refines

Two types of particles, *i.e.*, prepared by mechanical crushing of bulk $L1_2$ modified $(Al_{1-x}Me_x)_3Ti$ intermetallic compounds and directly prepared by gas atomization, were used [13-17]. Hereafter, the particles prepared by the crushing of an arc melted bulk sample and prepared by the gas atomization will be denoted as "crushed particles" and "gas-atomized particles", respectively. The bulk $L1_2$ modified $(Al_{1-x}Me_x)_3Ti$ intermetallic compound was prepared by an arc melting method under an argon atmosphere. The obtained bulk $(Al_{1-x}Me_x)_3Ti$ intermetallic compound was homogenized at elevated temperature, and then crushed into fine particles by a hammer. Both crushed and gas-atomized particles were sieved into the size of 75-150μm. The sieved $(Al_{1-x}Me_x)_3Ti$ particles are mixed with pure aluminum particles (99.9%, 106-180μm), where the volume fraction of $(Al_{1-x}Me_x)_3Ti$ particles was 10 vol%, 20 vol%, 30 vol% and 40 vol%. Sintering of the mixed powder using a spark plasma sintering (SPS) [23-25] was performed at 500 ^oC for 5 min under an applied stress of 45 MPa. Flow diagram for fabrication process of the refiners with $L1_2$ modified $(Al_{1-x}Me_x)_3Ti$ particles is shown in Fig. 3.

3.2 Refining Performance

To evaluate the grain refinement performance of the fabricated refiners containing $L1_2$ modified $(Al_{1-x}Me_x)_3Ti$ heterogeneous nucleation site particles, following casting experiments were conducted. Commercially pure aluminum ingot (99.99%, 148.8 g for 10 vol% refiner, 149.4 g for 20 vol% refiner, 149.6 g for 30 vol% refiner, and 149.7 g for 40 vol% refiner) was melted in an alumina crucible using the electrical resistance furnace at 750 °C in argon gas atmosphere. The mass fractions of the refiners as additives were 0.8%, 0.4%, 0.27% and 0.2% for the 10, 20, 30, and 40 vol% refiners, respectively, so that the total amount of

$L1_2$ modified $(Al_{1-x}Me_x)_3Ti$ particles within the melt was the same. After the addition of the refiner into the melt, the melt was stirred with a rod for 30 s, after which no further stirring was carried out. The melt was cast into a cylindrical steel mold of 45mm inner diameter, 70mm outer diameter, and 70mm height after a holding time. Here, the holding time is the time interval from when the stirring was finished to when the melt was cast into the mold. The classical metallographic route was used to prepare the samples for microstructural analysis. The specimen for grain structure examination was horizontally cut from the bottom part (5 mm from the bottom) of each cast sample. The macrostructural and microstructural features of the casts were studied by optical microscopy or scanning electron microscopy after etching the polished surface with a 10% hydrofluoric acid aqueous solution. Flow diagram of grain refining performance test is summarized in Fig. 4.

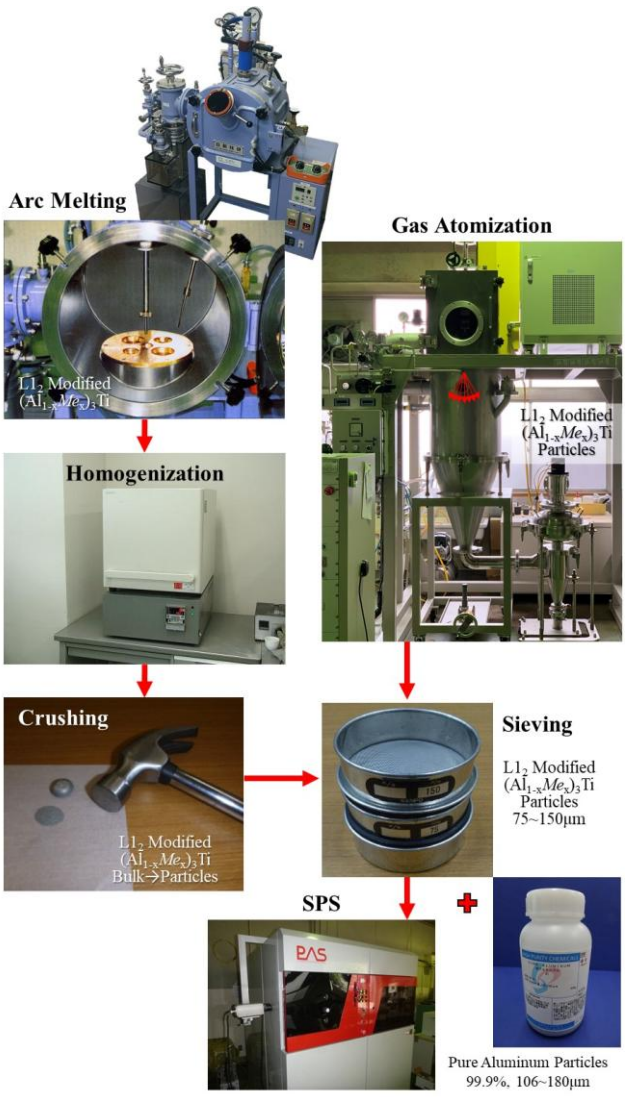

Fig. 3. Flow diagram for fabrication process of the refiners with $L1_2$ modified $(Al_{1-x}Me_x)_3Ti$ particles.

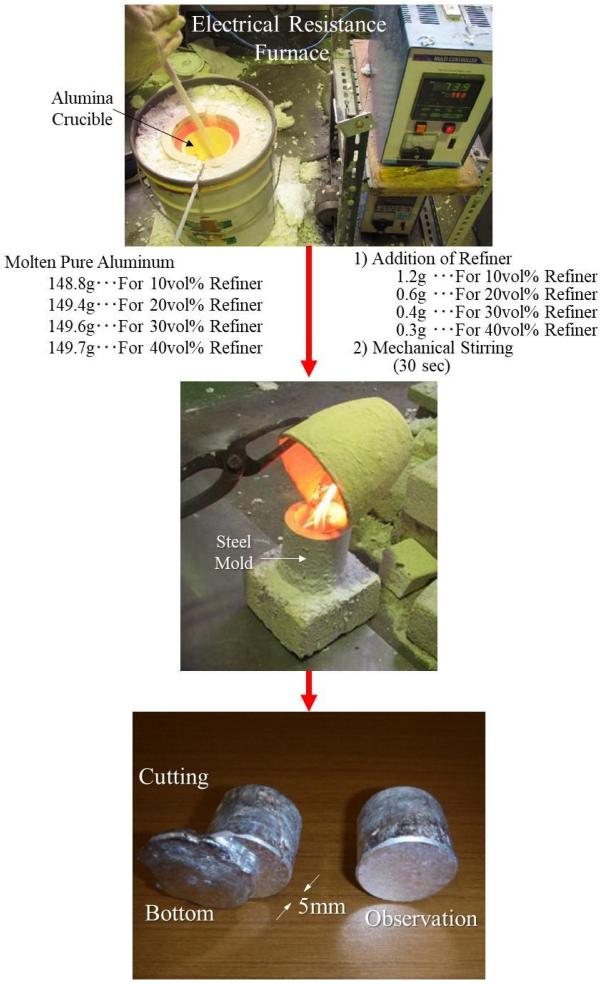

Fig. 4. Flow diagram for casting experiment of the refiners with $L1_2$ modified $(Al_{1-x}Me_x)_3Ti$ particles.

4 RESULTS AND DISCUSSION

4.1 Refined by Al-10 vol%$Al_{2.7}Fe_{0.3}Ti$

The SEM photomicrographs of Al-10 vol% $Al_{2.7}Fe_{0.3}Ti$ refiners with homogenized crushed particles and gas-atomized particles are shown in Figs. 5 (a) and (b), respectively [13]. It is seen that reaction between the $Al_{2.7}Fe_{0.3}Ti$ intermetallic compound and the aluminum matrix is not found at the interface, even though the refiners were fabricated by the sintering route. However, heating of Al-10 vol% $Al_{2.7}Fe_{0.3}Ti$ refiners with gas-atomized particles at 750°C for 300s causes microstructural evolution, as shown in Fig. 5 (c) [14]. The particles in the heated Al-10 vol% $Al_{2.7}Fe_{0.3}Ti$ refiners with gas-atomized particles have a core and mantle microstructure, and the chemical compositions of the core region and mantle region are a titanium rich $Al_{2.7}Fe_{0.3}Ti$ phase and $Al_3(Ti,Fe)$, respectively.

It is also visible from cross-sectional observations of gas-atomized particles (Fig. 5 (b)) that the gas-atomized particles contain a mesh-shaped secondary phase. However, such secondary phase is not found in the inside of the crushed particle as shown in Fig. 5 (a). Instead, secondary phase was found on the surface of

crushed particles. This may be evidence of the fragmentation behavior of the arc-melted intermetallic compound sample, caused by crushing with a hammer. Namely, fragmentation occurs across the secondary phase, and as a result, the secondary phase exists not in the inside of the crushed particle but on its surface. Anyhow, it can be concluded that the $L1_2$ modified $Al_{2.7}Fe_{0.3}Ti$ intermetallic compound particles can be successfully embedded in the aluminum matrix by SPS without any reaction.

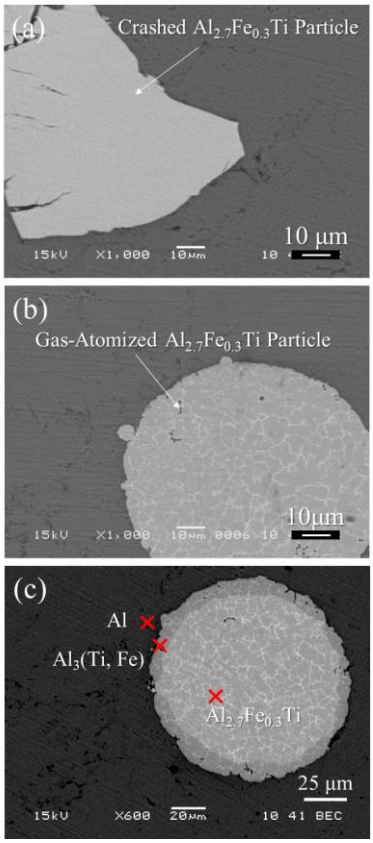

Fig. 5. SEM photomicrographs showing Al-10 vol% $Al_{2.7}Fe_{0.3}Ti$ refiners with (a) crushed particles and (b) gas-atomized particles before heating [13], and (c) after heating at 750°C for 300 s [14].

By using the Al-10 vol% $Al_{2.7}Fe_{0.3}Ti$ refiners with homogenized crushed particles and gas-atomized particles, the casting experiments are carried out, and the results are shown in Figs. 6 (b) and (c), respectively [13]. A photomacrograph taken before addition is shown in Fig. 6 (a). It is seen from Figs. 6 (a) to (c) that the higher grain refining efficiency is found for the refiner with gas-atomized particles compared with the refiner with homogenized crushed particles. This is because the secondary phase in the gas-atomized particles is mainly located inside the particles, while that in the crushed particles located on the surface of the particles, which may lead to large parameter *M* value of heterogeneous nucleation site particles.

The lattice matching between the particles and the solidified phase is critical to the effectiveness of the heterogeneous nucleation site. To discuss the effects of the lattice matching on the grain refining performance, the grain refining performance of the unhomogenized crushed refiner with a certain amount of the secondary phase on the surface of particles and heated gas-atomized refiner with partially decomposed $Al_{2.7}Fe_{0.3}Ti$ particles are studied. The results are also shown in Figs. 6 (d) and (e), respectively [14]. As can be seen, the grain-refining efficiency of the unhomogenized crushed refiner or heated gas-atomized refiner is inferior to that of the homogenized crushed refine or unheated refiner, respectively. This is because the surfaces of the unhomogenized crushed particles and heated particles are covered with secondary phase and mantle phases, which may have a lower lattice matching. Different refining performance characteristics appeared for refiners with different phases, even though the chemical compositions of the refiners themselves were the same.

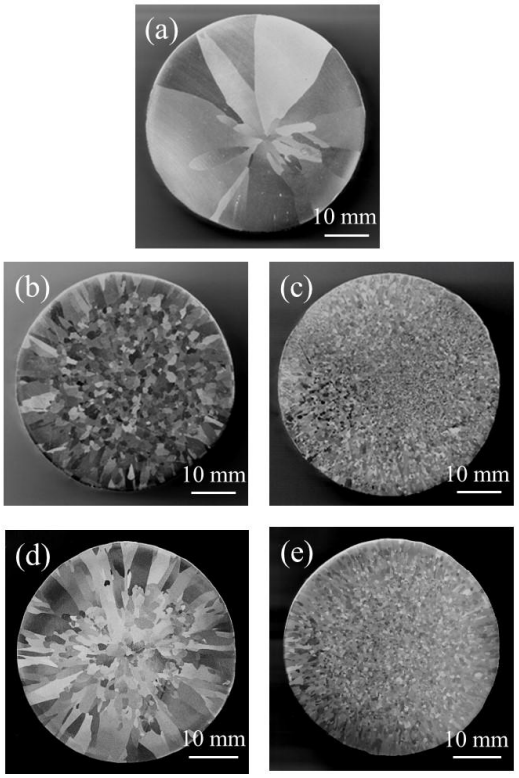

Fig. 6. Grain refining performance test results of the Al-10 vol% $Al_{2.7}Fe_{0.3}Ti$ refiner with (b) crushed particles and (c) gas-atomized particles [13]. A photomacrograph taken before addition is also shown in (a). Results of (d) unhomogenized Al-10 vol% $Al_{2.7}Fe_{0.3}Ti$ refiner and (e) heated Al-10 vol% $Al_{2.7}Fe_{0.3}Ti$ refiner [14]. Holding time of the grain refining performance test is 600 s.

4.2 Refined by Al-(10-40)vol%$Al_{2.5}Cu_{0.5}Ti$

SEM micrographs of the Al-10vol%, 20 vol%, 30 vol% and 40 vol% $Al_{2.5}Cu_{0.5}Ti$ refiners with gas-atomized particles are shown in Figs. 7 (a) to (d), respectively [16]. Spherical shaped gas-atomized particles are homogeneously distributed in the aluminum matrix, even when there is a high volume fraction of refiner. The SPS process thus successfully produced fully dense refiners consisting of a high volume fraction of $Al_{2.5}Cu_{0.5}Ti$ particles embedded in the aluminum matrix.

The refiners containing different amounts of heterogeneous nucleation site particles showed differences in the grain refining performance with the holding time, even though the total amount of $Al_{2.5}Cu_{0.5}Ti$ particles within the melt was the same. The best holding times for the 10 vol%, 20 vol%, 30 vol%, and 40 vol% atomization refiners were determined to be 300 s, 420 s, 540 s and 600 s, respectively. The results of grain refinement performance tests for the 10 vol%, 20 vol%, 30vol% and 40 vol% atomization refiners with holding times of 300 s, 420 s, 540 s and 600 s are shown in Figs. 8 (a) to (d), respectively [16]. Longer holding time is required to achieve a uniform dispersion of $Al_{2.5}Cu_{0.5}Ti$ particles in the melt for the refiners with high volume fraction of heterogeneous nucleation site particles. In this way, fading of the grain refinement effect occurs slower when the volume fraction of heterogeneous nucleation site particles increased.

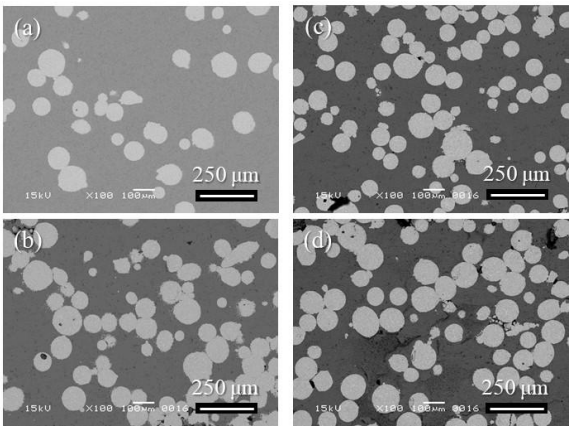

Fig. 7. SEM micrographs of fabricated (a) Al-10vol%, (b) 20 vol%, (c) 30 vol% and (d) 40 vol% $Al_{2.5}Cu_{0.5}Ti$ refiners with gas-atomized particles [16].

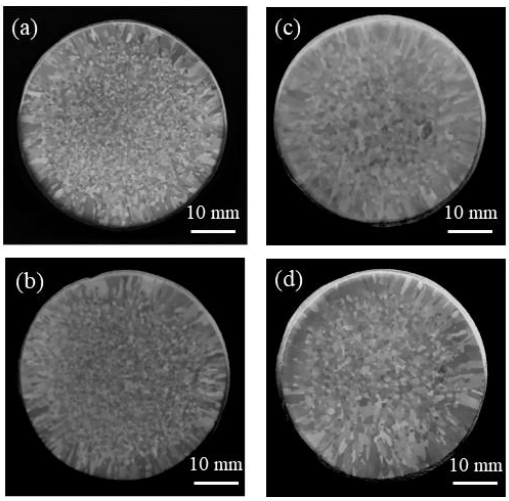

Fig. 8. Macrostructures of aluminum casts refined with (a) Al-10vol%, (b) 20 vol%, (c) 30 vol% and (d) 40 vol% $Al_{2.5}Cu_{0.5}Ti$ refiners with gas-atomized particles by hold times of 300 s, 420 s, 540 s and 600 s, respectively [16]. The levels of addition were 0.8%, 0.4%, 0.27% and 0.2% for the 0, 20, 30, and 40 vol% atomization refiners, respectively, so that the total amount of $Al_{2.5}Cu_{0.5}Ti$ particles within the melt was the same.

4.3 Refined by Al-10 vol%$Al_{2.7}Ni_{0.3}Ti$

The minimum grain size can be achieved for the cast refined by the Al-10 vol% $Al_{2.7}Ni_{0.3}Ti$ refiner after the holding time of 690 s, as shown in Fig. 9 (a) [15]. This size is about one ninth that of the unrefined cast. However, a lower grain refinement efficiency is found for the Al-10 vol% $Al_{2.7}Ni_{0.3}Ti$ refiner than for the Al-10 vol% $Al_{2.7}Fe_{0.3}Ti$ refiner shown in Fig. 6 (c). This phenomenon cannot be explained by simple lattice matching between the heterogeneous nucleation site and the solidified phase, since the M value between $Al_{2.7}Ni_{0.3}Ti$ and aluminum, $M = 1.93 \times 10^{-3}$, is smaller than that between $Al_{2.7}Fe_{0.3}Ti$ and aluminum, 2.50×10^{-3}.

Next, the thermal stability of the $Al_{2.7}Ni_{0.3}Ti$ phase in the Al-10 vol% $Al_{2.7}Ni_{0.3}Ti$ refiner was investigated. For this purpose, the Al-10 vol% $Al_{2.7}Ni_{0.3}Ti$ refiner was heated at 750 ^{o}C for 300 s, and result is shown in Fig. 9 (b) [15]. It is seen that heating for a short time causes the decomposition of the $Al_{2.7}Ni_{0.3}Ti$ phase into Al_3Ti and Al_3Ni phases. On the other hand, in the case of the heated Al-10 vol% $Al_{2.7}Ni_{0.3}Ti$ refiner, the particles have a core and mantle microstructure as shown in Fig. 5 (c), and the chemical composition of the core region is still $Al_{2.7}Fe_{0.3}Ti$ phase. By comparing the decomposition phenomena in the Al-10 vol% $Al_{2.7}Ni_{0.3}Ti$ and Al-10 vol% $Al_{2.7}Fe_{0.3}Ti$ refiners, it is found that the thermal stability of the $Al_{2.7}Ni_{0.3}Ti$ phase in the refiner is lower than that of the $Al_{2.7}Fe_{0.3}Ti$ phase. This may be the reason for the relatively lower grain refinement performance of the Al-10 vol% $Al_{2.7}Ni_{0.3}Ti$ refiner. In this way, the thermal stability of the heterogeneous nucleation site also affects the grain refinement performance.

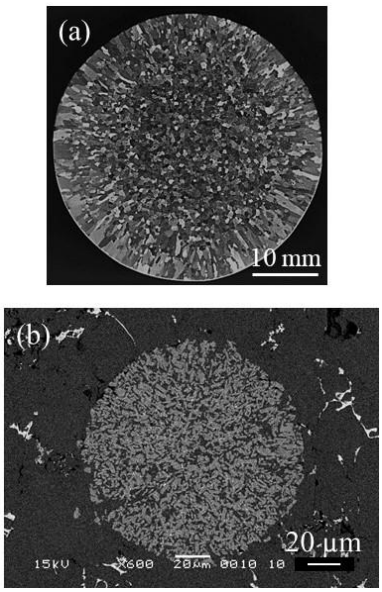

Fig. 9. (a) Grain refinement performance test result of the Al-10 vol% $Al_{2.7}Ni_{0.3}Ti$ refiner after holding time of 690 s. (b) Microstructure of Al-10 vol% $Al_{2.7}Ni_{0.3}Ti$ refiner heated at 750 ^{o}C for 300 s [15].

5 CONCLUSIONS

In this paper, the role of $L1_2$ modified $(Al_{1-x}Me_x)_3Ti$ phases on the heterogeneous nucleation of alpha aluminum primary crystal was reviewed. The refiners with $L1_2$ modified $(Al_{1-x}Me_x)_3Ti$ particles prepared by gas atomization or crushing were fabricated by SPS. The results are summarized as follows.

1) $L1_2$ modified $(Al_{1-x}Me_x)_3Ti$ particles can be prepared by mechanical crushing of bulk $L1_2$ modified $(Al_{1-x}Me_x)_3Ti$ intermetallic compounds and directly prepared by gas atomization. The $L1_2$ modified $(Al_{1-x}Me_x)_3Ti$ particles embedded in an aluminum matrix do not react with aluminium nor transformation into stable phases during sintering.

2) The aluminum cast without the refiner has coarse and inhomogeneous grains. On the other hand, the grain size is smaller in the aluminum cast with the Al-$(Al_{1-x}Me_x)_3Ti$ refiners. Therefore, $L1_2$ modified $(Al_{1-x}Me_x)_3Ti$ particles can act as effective heterogeneous nucleation sites for primary aluminum in the solidification process.

3) Different refining performance characteristics appeared for refiners with different phases, even though the chemical compositions of the refiners themselves were the same. This is because the lattice matching between heterogeneous nucleation site particles and solidified aluminum is critical to obtain finer grain structures for aluminum casts.

4) Although $L1_2$ modified $Al_{2.7}Ni_{0.3}Ti$ phase has small M value, the grain refinement performance of Al-10 vol% $Al_{2.7}Ni_{0.3}Ti$ refiner is relatively weaker than expected. This is because the Al-10 vol% $Al_{2.7}Ni_{0.3}Ti$ refiner does not have a high thermal stability. The thermal stability of the heterogeneous nucleation site also affects the grain refinement performance.

This work was supported by The Light Metal Educational Foundation Inc. of Japan, the New Energy and Industrial Technology Development Organization (NEDO) of Japan and Japan Science and Technology Agency (JST) ‘‘Collaborative Research Based on Industrial Demand’’ Grand Number JPMJSK1614.

References

1. P. S. Mohanty, J. E. Gruzleski, Acta Mater., **43**, No. 5, 2001 (1995).
2. B. S. Murty, S. A. Kori, K. Venkateswarlu, R. R. Bhat, M. Chakraborty, J. Mater. Proc. Tech., **89-90**, 152 (1999).
3. Y. Watanabe, N. Yamanaka, Y. Fukui, Z. Metallkd., **88**, No. 9, 717 (1997).
4. Y. Watanabe, N. Yamanaka, Y. Fukui, Metall. Mater. Trans. A, **30A**, No. 12, 3253 (1999).
5. Y. Watanabe, H. Eryu, K. Matsuura, Acta Mater., **49**, No. 5, 775 (2001).
6. P. D. Sequeira, Y. Watanabe, Y. Fukui, Scrip. Mater., **53**, No. 6, 687 (2005).
7. P. D. Sequeira, Y. Watanabe, H. Eryu, T. Yamamoto, K. Matsuura, Trans. ASME, J. Eng. Mater.Tech., **129**, No. 2, 304 (2007).H. Sato, Y. Noda, Y. Watanabe, Mater. Trans., **54**, No. 8, 1274, (2013).
8. Y. Watanabe, P. D. Sequeira, H. Sato, T. Inamura, H. Hosoda, Jpn J. Appl. Phys., **55**, No. 1, 01AG03 (2016).
9. J. Tarnacki, Y.-W. Kim, Scr. Metall., **22**, No. 3, 329 (1988).
10. H. Mabuchi, K. Hirukawa, H. Tsuda, Y. Nakayama, Scr. Metall. Mater., **24**, No. 3, 505 (1990).
11. Y. Nakayama, H. Mabuchi, Intermetallics, **1**, No. 1, 41 (1993).
12. Y. Watanabe, K. Hirata, H. Sato, Jpn J. Appl. Phys., **57**, No. 1S, 01AF04 (2018).
13. Y. Watanabe, T. Hamada, H. Sato, Jpn J. Appl. Phys., **55**, No. 1, 01AG01 (2016).
14. Y. Watanabe, T. Hamada, H. Sato, Jpn J. Appl. Phys., **56**, No. 1S, 01AG02 (2017).
15. Y. Watanabe, K. Maekawa, H. Sato, Jpn J. Appl. Phys., **57**, No. 1S, 01AF08 (2018).
16. Y. Watanabe, R. Yamazaki, K. Yamanaka, H. Sato, J. Mater. Proc. Tech., **255**, 400 (2018) .
17. Y. Watanabe, S. Taniai, H. Sato, Jpn J. Appl. Phys., **58**, No. SA, SAAC04 (2019).
18. D. Turnbull, B. Vonnegut, Ind. Eng. Chem., **44**, No. 6, 1292 (1952).
19. B. L. Bramfitt, Metall. Trans., **A 1**, No. 7, 1987 (1970).
20. M. Kato, M. Wada, A. Sato, T. Mori, Acta Metal., **37**, No. 3, 749 (1989).
21. Y. Watanabe, Q. Zhou, H. Sato, T. Fujii, T. Inamura, Jpn J. Appl. Phys., **56**, No. 1S, 01AG01 (2017).
22. Y. Watanabe, M. Sato, T. Chiba, H. Sato, N. Sato, S. Nakano, Metall. Mater. Trans. A, **51A**, No. 3, 1345 (2020).
23. U. Anselmi-Tamburini, J.E. Garaya, Z.A. Munira, Mater. Sci. Eng. A, **407**, 24 (2005).
24. M. Omori, Mater. Sci. Eng. A, **287**, 183 (2000).
25. Y. Watanabe, Y. Iwasa, H. Sato, A. Teramoto, K. Abe, E.Miura-Fujiwara, J. Mater. Proc. Tech., **211**, 1919 (2011).